Cell

TRIP12 and UBR5 Suppress Spreading of Chromatin Ubiquitylation at Damaged Chromosomes

Thorkell Gudjonsson,[1,7] Matthias Altmeyer,[1,7] Velibor Savic,[1] Luis Toledo,[1] Christoffel Dinant,[2] Merete Grøfte,[1] Jirina Bartkova,[2] Maria Poulsen,[3] Yasuyoshi Oka,[3] Simon Bekker-Jensen,[3] Niels Mailand,[3] Beate Neumann,[4] Jean-Karim Heriche,[4] Robert Shearer,[5] Darren Saunders,[5] Jiri Bartek,[2,6] Jiri Lukas,[1,3,*] and Claudia Lukas[1]

[1]Chromosome Biology Unit

[2]Genome Integrity Unit

Danish Cancer Society Research Center and Center for Genotoxic Stress Research, Strandboulevarden 49, DK-2100 Copenhagen, Denmark

[3]Novo Nordisk Foundation Center for Protein Research, University of Copenhagen, Blegdamsvej 3B, DK-2200 Copenhagen, Denmark

[4]European Molecular Biology Laboratory, Meyerhofstrasse1, D-69117 Heidelberg, Germany

[5]Cancer Research Program, Garvan Institute of Medical Research and St. Vincent's Clinical School, Faculty of Medicine, University of New South Wales, 384 Victoria Street, Darlinghurst NSW 2010, Australia

[6]Institute of Molecular and Translational Medicine, Faculty of Medicine, Palacky University, CZ-775 15 Olomouc, Czech Republic

[7]These authors contributed equally to this work

*Correspondence: jiri.lukas@cpr.ku.dk

http://dx.doi.org/10.1016/j.cell.2012.06.039

SUMMARY

Histone ubiquitylation is a prominent response to DNA double-strand breaks (DSBs), but how these modifications are confined to DNA lesions is not understood. Here, we show that TRIP12 and UBR5, two HECT domain ubiquitin E3 ligases, control accumulation of RNF168, a rate-limiting component of a pathway that ubiquitylates histones after DNA breakage. We find that RNF168 can be saturated by increasing amounts of DSBs. Depletion of TRIP12 and UBR5 allows accumulation of RNF168 to supraphysiological levels, followed by massive spreading of ubiquitin conjugates and hyperaccumulation of ubiquitin-regulated genome caretakers such as 53BP1 and BRCA1. Thus, regulatory and proteolytic ubiquitylations are wired in a self-limiting circuit that promotes histone ubiquitylation near the DNA lesions but at the same time counteracts its excessive spreading to undamaged chromosomes. We provide evidence that this mechanism is vital for the homeostasis of ubiquitin-controlled events after DNA breakage and can be subverted during tumorigenesis.

INTRODUCTION

Histone ubiquitylation is an integral part of intertwined pathways that build up the DNA damage epigenome (Lukas et al., 2011b). It is triggered by RNF8, a RING finger E3 ligase that initiates ubiquitylation of H2A and H2AX. These priming ubiquitin reactions are edited by p97 segregase (Acs et al., 2011; Meerang et al., 2011) and are amplified by RNF168, another RING finger E3 ligase. The resulting lysine-63-linked ubiquitin polymers generate an interaction platform for chromatin-associated repair and signaling factors, including 53BP1 and the RAP80/BRCA1 complex (Bothmer et al., 2010, 2011; Bouwman et al., 2010; Bunting et al., 2010; Coleman and Greenberg, 2011; Hu et al., 2011). In addition, RNF8/RNF168-mediated ubiquitylation of H2A inhibits messenger RNA (mRNA) elongation, a mechanism that has likely evolved to avoid collisions between transcription and repair intermediates (Shanbhag et al., 2010). Chromatin ubiquitylation also facilitates fusion of uncapped telomeres (Peuscher and Jacobs, 2011), which can be viewed as a cellular strategy to survive telomere attrition. Moreover, chromatin ubiquitylation is required for formation of the G1 nuclear bodies that shield DNA lesions generated during mitosis on genomic loci exposed to replication stress (Harrigan et al., 2011; Lukas et al., 2011a).

Apart from these positive impacts on genome stability, the biochemical properties of RNF168 pose a potential threat; by combining a catalytic RING domain and several ubiquitin-binding domains within its structure (Doil et al., 2009; Pinato et al., 2011; Stewart et al., 2009), RNF168 can amplify ubiquitin conjugates generated by its own activity. Hence, once recruited to the sites of DNA damage, RNF168 is poised to progressively spread away from the DNA double-strand break (DSB) to undamaged chromatin. An uncontrolled amplification of chromatin ubiquitylation could have deleterious consequences, including unscheduled transcriptional silencing, or sequestering cellular pools of limiting genome caretakers. Thus, an outstanding conundrum is how cells control that these profound epigenetic alterations remain confined to the sites of DNA damage.

To control DNA-damage-induced chromatin ubiquitylations, cells mobilize at least three deubiquitylating enzymes (DUBs), BRCC36, USP3, and OTUB1, respectively (Doil et al., 2009; Nakada et al., 2010; Nicassio et al., 2007; Shao et al., 2009).

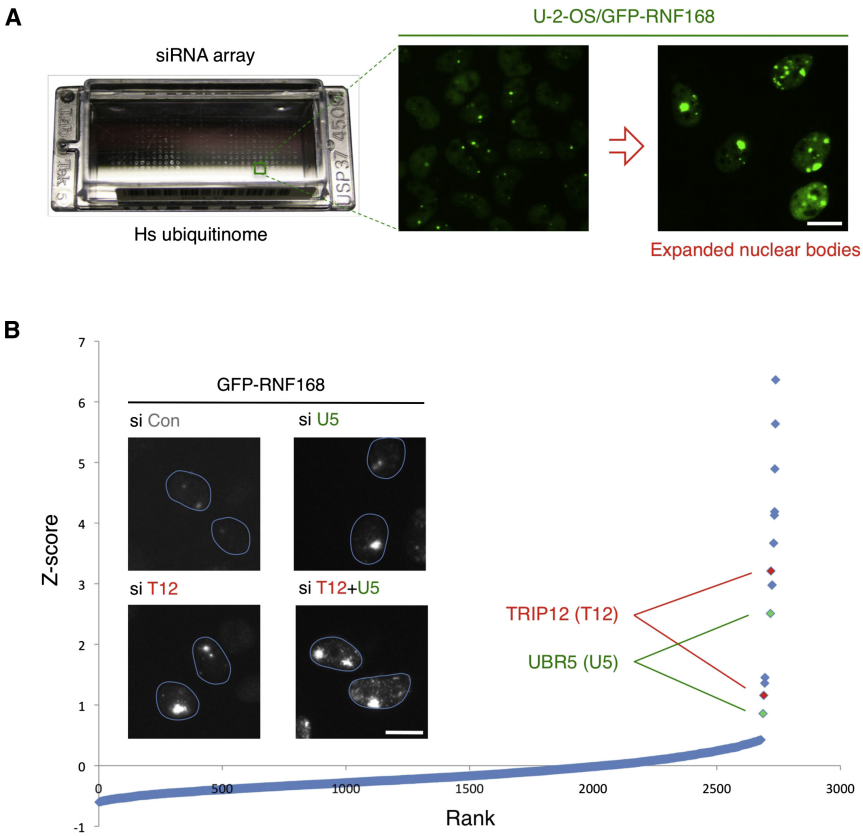

C

Top hits*

TRIP12	PSMA1-3, 4, 7
UBR5	PSMB 1-7
UBE2D3	PSMC1, 4, 6
UBE2L3	PSMD1, 2, 6-8, 11, 12
RPL5	POMP
RBM8A	SF3A3
BIRC2	GNBL1
TRAF3	

*Genes whose knockdown by two independent siRNAs increased expansion of GFP-RNF168-decorated nuclear bodies

Figure 1. Identification of TRIP12 and UBR5 as Regulators of Chromatin Ubiquitylation at Spontaneous DNA Lesions

(A) A schematic depiction of the screening procedure combining siRNA arrays spanning the human ubiquitinome and a readout based on monitoring the increase of the GFP-RNF168-associated fluorescence at the G1 nuclear bodies.

(B) A scatterplot of Z-scores derived from the screen shown in (A). Insets show representative images from manual re-examination of nuclear body expansion in U-2-OS/GFP-RNF168 cells treated with the indicated siRNAs; henceforth, siRNA is abbreviated as si, Control as Con, and TRIP12 and UBR5 as T12 and U5, respectively.

(C) List of genes whose knockdown by two independent siRNA increased the expansion of GFP-53BP1-decorated nuclear bodies.

Scale bars, 10 μm. See also Table S1.

Although all these DUBs can counteract the activity of RNF168/UBC13 holoenzyme, it is not clear whether they can fully control the pathway once the amplification step catalyzed by RNF168 is set in motion. For instance, it remains to be determined whether these or other DUBs generate a constant "threshold" that needs to be overcome by RNF168 or whether their activities are turned on only to terminate chromatin ubiquitylation upon completion of DNA repair.

To gain insight into the spatial regulation of stress-induced chromatin ubiquitylations, we screened the human ubiquitinome for suppressors of RNF168 and identified TRIP12 and UBR5, two HECT domain E3 ligases implicated previously in a broad range of physiological processes, including N-end rule proteolysis and ubiquitin fusion degradation (Varshavsky, 2011), elimination of proteins uncoupled from their physiological interactors (Chen et al., 2010; Keppler and Archer, 2010; Park et al., 2008), cell-cycle checkpoints (Henderson et al., 2006; Munoz et al., 2007), and cotranslational protein quality control (Pegoraro et al., 2012). Our results reveal an unexpected function of TRIP12 and UBR5 in delineating the dynamic range for RNF168 accumulation and thereby rendering the DNA-damage-induced histone ubiquitylation intrinsically self limiting. We show that this mechanism is used by cells to coordinate repair dynamics and to avoid excessive transcriptional silencing.

RESULTS

Identification of TRIP12 and UBR5 as Regulators of RNF168

To identify factors that limit the DNA-damage-induced histone ubiquitylation, we cultured U-2-OS cells stably expressing green fluorescent protein (GFP)-RNF168 on small interfering RNA (siRNA) arrays targeting the known human ubiquitinome (Moudry et al., 2012), and we screened for genes whose knockdown by at least two independent siRNAs increased GFP-RNF168 accumulation on the G1 nuclear bodies formed around spontaneous DNA lesions (Figure 1A). Prominent among the positive hits were the structural and catalytic subunits of the 26S proteasome (Figures 1B and 1C and Table S1 available online), indicating that unscheduled protein accumulation enhances histone ubiquitylation. Interestingly, out of all E3 ligases included in the siRNA arrays, only TRIP12 and UBR5 recapitulated this phenotype (Figures 1B and 1C), and their simultaneous knockdown showed an additive effect in expanding the nuclear

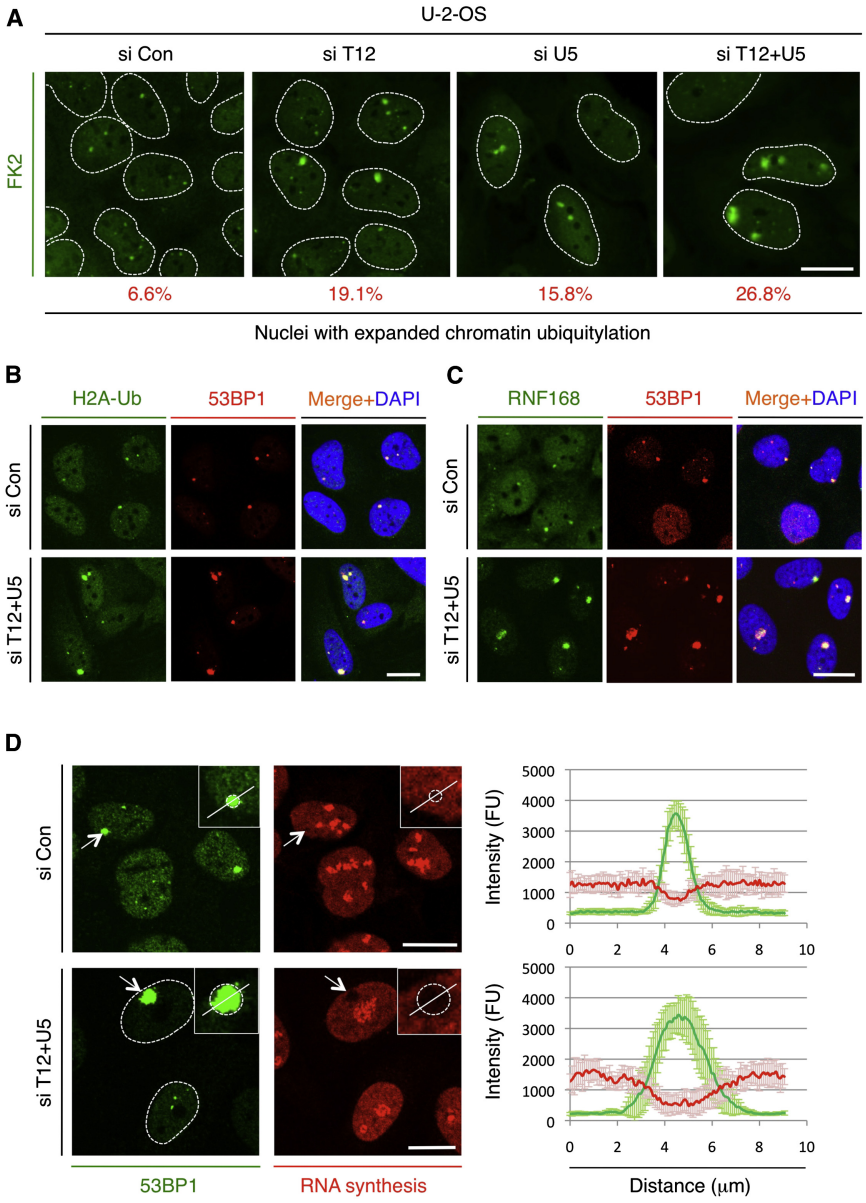

Figure 2. Expansion of the Ubiquitylated Nuclear Domains in TRIP12- and UBR5-Depleted Cells Is Accompanied by Reduced Transcription

(A) U-2-OS cells were transfected with the indicated siRNAs for 72 hr and immunostained with the FK2 antibody against conjugated ubiquitin. Numbers indicate the fraction of nuclei with enlarged ubiquitin-decorated nuclear bodies (larger than 80 pixels). For each condition, a randomly selected cohort of at least 500 cells was analyzed. One pixel, 0.2 × 0.2 μm.

(B) U-2-OS cells were transfected with the indicated siRNAs for 72 hr and immunostained with antibodies to 53BP1 and ubiquitylated H2A.

(C) U-2-OS cells were transfected with siRNAs as in (B) and immunostained with antibodies to 53BP1 and RNF168.

(D) U-2-OS cells were transfected with the indicated siRNAs for 72 hr, incubated in the presence of 5-ethinyl uridin (5-EU) for the last 1 hr, and immunostained with antibodies to 53BP1. The 5-EU incorporation to nascent mRNA was developed with Click-iT chemistry. The fluorescence intensity profiles were quantified along a line drawn through the center of the nuclear bodies. Insets show larger magnification of nuclear bodies; graphs integrate data from ten cells for each condition. Error bars represent SD.

Scale bars, 10 μm. See also Figure S1.

territory occupied by GFP-RNF168 (Figure 1B). Thus, TRIP12 and UBR5 emerge as suppressors of RNF168.

TRIP12 and UBR5 Determine the Spreading of Chromatin Ubiquitylation and Transcriptional Silencing after DNA Damage

Fluorescence quantifications performed in naive U-2-OS cells confirmed and extended the screening data by showing that the knockdown of TRIP12 and UBR5 had an additive effect on inducing large G1 nuclear bodies enriched in ubiquitin conjugates (Figure 2A), including ubiquitylated H2A and H2AX, the known targets of RNF168 (Figures 2B and S1A). These expanded nuclear compartments accumulated endogenous RNF168 itself (Figure 2C), as well as the established chromatin-associated ubiquitin sensors RAP80, BRCA1, and 53BP1 (Figures 2C, S1B, and S1C), but not RNF8 (Figure S1D). The expansion phenotypes were reproduced by multiple siRNAs (Figures S2A and S2B) and are seen also in primary human fibroblasts (Figure S3A).

We excluded that the observed phenotypes were caused by unspecific protein aggregation. As we show in Figure S3B, the expanded G1 nuclear bodies remained highly dynamic and preserved cell-cycle periodicity as their normal-sized counterparts (Lukas et al., 2011a). In addition, disruption of the upstream regulators of chromatin ubiquitylation (inhibition of ataxia telangiectasia mutated [ATM] and knockdown of MDC1 or RNF8, respectively) abolished 53BP1 focus formation after combined depletion of TRIP12 and UBR5 (Figures S3C and S3D), suggesting that the signaling generated at the DSB sites is continuously required to support RNF168 recruitment and the ensuing spreading.

To explore whether the enlargement of the ubiquitin-enriched chromatin domains entails functional consequences, we exploited the recent findings that the DSB-induced chromatin ubiquitylations inhibit mRNA elongation (see Introduction). Indeed, by combining immunostaining of 53BP1 with in situ detection of nascent mRNA, we observed a marked reduction of de novo mRNA synthesis throughout the expanded chromatin domains (Figure 2D). Together, these data indicate that depletion of

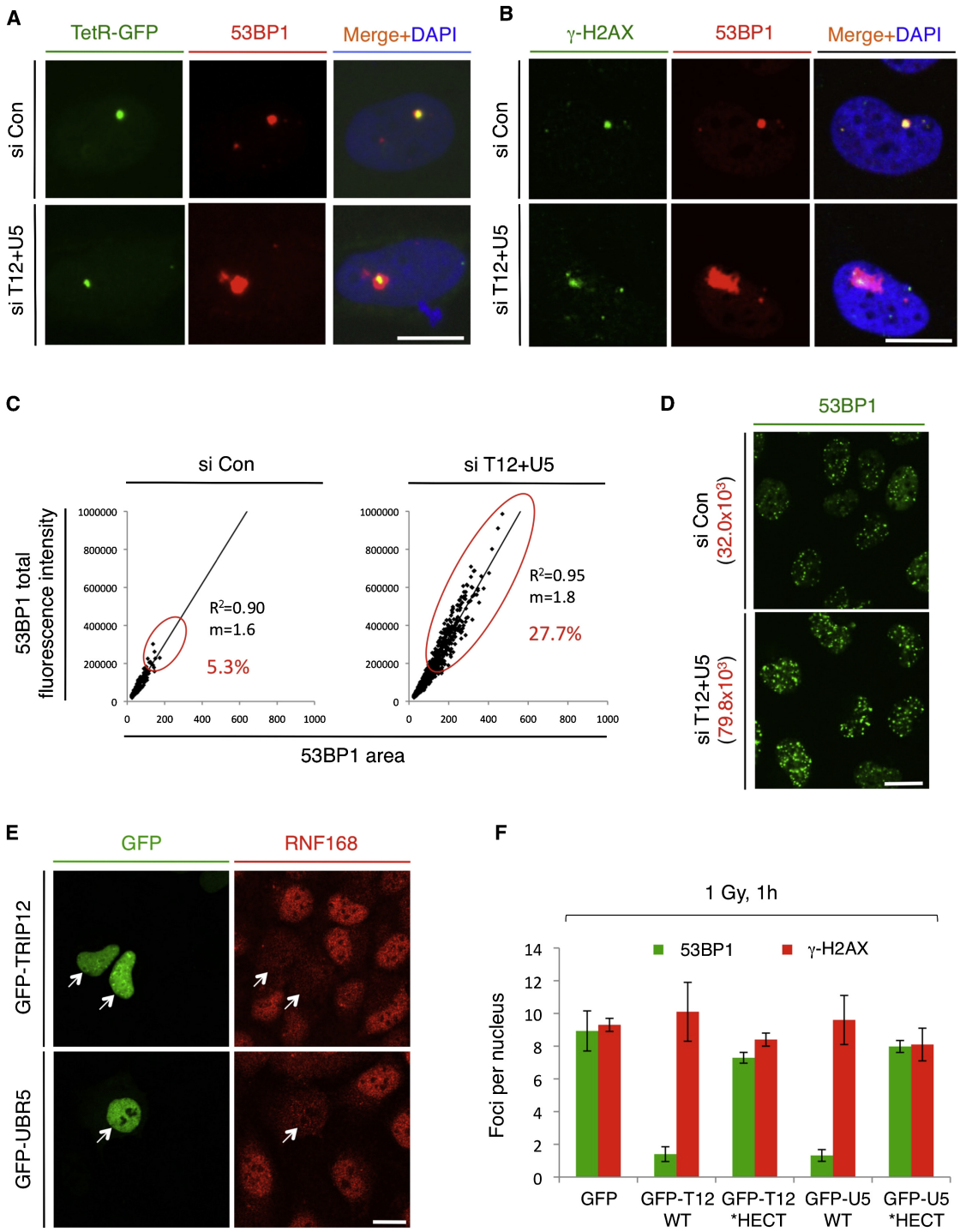

Figure 3. Catalytic Activities of TRIP12 and UBR5 Regulate Ubiquitin Spreading, but Not Chromatin Decondensation, after DNA Damage

(A) U-2-OS-TetO cells harboring 240 TetO repeats next to the I-SceI restriction site were transfected with the indicated siRNAs, induced to cut the I-SceI site, and immunostained with antibodies to 53BP1; the locus with integrated TetO repeats was visualized by transient transfection of TetR-GFP.

(B) U-2-OS cells were transfected with the indicated siRNAs for 72 hr and immunostained with the indicated antibodies.

(C) Total fluorescence intensities of 53BP1 nuclear bodies were plotted against 53BP1 nuclear body areas. Coefficient of determination of a linear regression (R^2) and the slope of the linear regression are provided for each condition. The fraction of 53BP1 nuclear bodies with an area greater than 100 pixels is indicated. For each condition, a randomly selected cohort of at least 300 cells was analyzed. One pixel, 0.2 × 0.2 μm.

(D) U-2-OS cells were transfected with the indicated siRNAs for 72 hr, exposed to IR (0.25 Gy), and 45 min later, were immunostained with an antibody to 53BP1. A randomly selected cohort of 500 cells was analyzed; numbers indicate total fluorescence intensity per 53BP1 focus.

TRIP12 and UBR5 allows unusually vast expansion of RNF168-catalyzed events accompanied by pronounced transcriptional silencing.

Importantly, the RNF8/RNF168 pathway functionally interacts with ATP-dependent chromatin remodelers (Lukas et al., 2011b), and thus, one way the expansion of the nuclear bodies can occur is via chromatin decompaction. However, at least three pieces of evidence suggested that the phenotypes observed in TRIP12/UBR5-depleted cells reflect an excessive spreading of ubiquitin conjugates. First, the combined TRIP12/UBR5 depletion triggered 53BP1 accumulation beyond the fluorescently labeled genomic loci cleaved by an I-SceI endonuclease (Figure 3A). Second, unlike the ubiquitin-dependent chromatin alterations, γ-H2AX did not expand beyond its normal range (Figure 3B). Third, the 53BP1-associated fluorescence intensity increased proportionally with the expanding nuclear body areas, again supporting the spreading scenario rather than diluting the density of ubiquitylated histones due to chromatin decondensation (Figure 3C). Collectively, these data suggest that depletion of TRIP12 and UBR5 uncouples histone phosphorylation and ubiquitylation by allowing the latter to spread beyond its physiological boundaries.

Mechanisms of TRIP12- and UBR5-Mediated Suppression of Chromatin Ubiquitylation

Because the G1 nuclear bodies can be viewed as compartments with specialized functions (Harrigan et al., 2011; Lukas et al., 2011a), we tested the impact of TRIP12/UBR5 knockdown also on bona fide clastogen-induced DSBs. Indeed, after exposing TRIP12/UBR5-depleted cells to low doses of ionizing radiation (IR), we observed a marked enhancement (size and intensity) of 53BP1 foci (Figures 3D and S3A). Conversely, overexpression of TRIP12 or UBR5 degraded endogenous RNF168 (Figure 3E), which was accompanied by suppression of IR-induced 53BP1 focus formation in a catalytic-dependent fashion (Figure 3F). Thus, active TRIP12 and UBR5 E3 ligases are required to suppress excessive chromatin ubiquitylations at IR-induced DSBs.

To dissect how TRIP12 and UBR5 cooperate to regulate the DNA-damage-induced ubiquitylation pathway, we analyzed the abundance of its catalytic components. As shown in Figure 4A, knockdown of UBR5 moderately increased the levels of all three E3 ligases involved in this pathway—RNF8, RNF168, and BRCA1, respectively. This is consistent with the recent identification of UBR5 as a general component of cotranslational protein quality surveillance (Pegoraro et al., 2012) and indicates that the key catalytic components of genotoxic stress-induced chromatin ubiquitylation are subjected to such regulation.

In contrast to UBR5, knockdown of TRIP12 triggered a massive accumulation specifically of RNF168, a phenotype reproduced by independent siRNAs (Figure S2B) and observed regardless of exogenous DNA damage (Figure 4A). Consistently, TRIP12 overexpression induced polyubiquitylation of RNF168 in cells (Figure S4A). The latter assay was performed with a catalytically inactive RNF168 excluding an indirect role of RNF168 autoubiquitylation. As mentioned in the Introduction, TRIP12 often targets proteins that are uncoupled from stoichiometric interactors, and we obtained evidence that such a mechanism may also apply for RNF168. Specifically, we have reported that silencing of HERC2, an established RNF168-binding protein, markedly destabilized RNF168 (Bekker-Jensen et al., 2010). As we show here, downregulation of RNF168 induced by HERC2 depletion could be mitigated by depletion of TRIP12 (Figure 4B). Importantly, a protein degradation assay based on measuring the decay of photoactivated GFP-RNF168 directly in living cells also revealed the cooperative effect of TRIP12 and UBR5 in regulating RNF168 turnover and confirmed the dominant role of TRIP12 in the process (Figure 4C).

In all of these assays, the cellular pool of free ubiquitin was not limiting (Figures S4B–S4D). Furthermore, although depletion of USP3 or RNF169, two established regulators of RNF168-controlled events (Doil et al., 2009; Poulsen et al., 2012), increased 53BP1 foci intensity, this effect was consistently less pronounced compared to depletion of TRIP12 and UBR5 (Figure S4E), pointing to a dominant role of TRIP12 and UBR5 in suppressing excessive RNF168-mediated chromatin ubiquitylation. Thus, whereas both TRIP12 and UBR5 can be copurified with ectopically expressed RNF168 to a similar extent (Figure S5A), the regulation of chromatin ubiquitylation by these E3 ligases appears to entail two complementary mechanisms. Whereas UBR5 seems to control accumulation of all major pathway components, TRIP12 likely represents a major specificity factor that guards against excessive RNF168 in cell nuclei. Finally, all of the above-described regulations operate strictly at the level of protein stability because neither single nor combined knockdown of TRIP12 and UBR5 affected RNF168 mRNA levels (Figure S5B).

Stabilization and Enhanced Chromatin Loading of RNF168 Are the Main Mediators of Ubiquitin Spreading at Damaged Chromatin

After TRIP12 and UBR5 depletion, the hyperaccumulation of RNF168 was followed by its increased loading on chromatin (Figure 4D). In contrast, we could not detect enhanced chromatin loading of RNF8 (Figure S5C), suggesting that the expansion of the ubiquitylated chromatin relies on RNF168. In support of this conclusion, overexpression of RNF168, but not RNF8 or BRCA1, was sufficient to expand chromatin domains around spontaneous DNA lesions marked by 53BP1 (Figure 4E; C.L. and J.L., our unpublished data). In addition, RNF8 did not expand beyond its normal chromatin territory in

(E) U-2-OS cells were transfected with the expression plasmids for GFP-TRIP12 or GFP-UBR5, incubated for 24 hr, and immunostained with an antibody to RNF168. Arrows mark the transfected cells.

(F) U-2-OS cells were transfected with the indicated expression plasmids; asterisks indicate an inactivating point mutation in the catalytic HECT domain. After 24 hr, cells were irradiated (1 Gy) and were immunostained 1 hr later as indicated, and the GFP-positive nuclei in each condition were scored for numbers of 53BP1 and γ-H2AX foci, respectively. The graph is a summary from three independent experiments.

Scale bars, 10 μm; error bars represent SD. See also Figures S3 and S4.

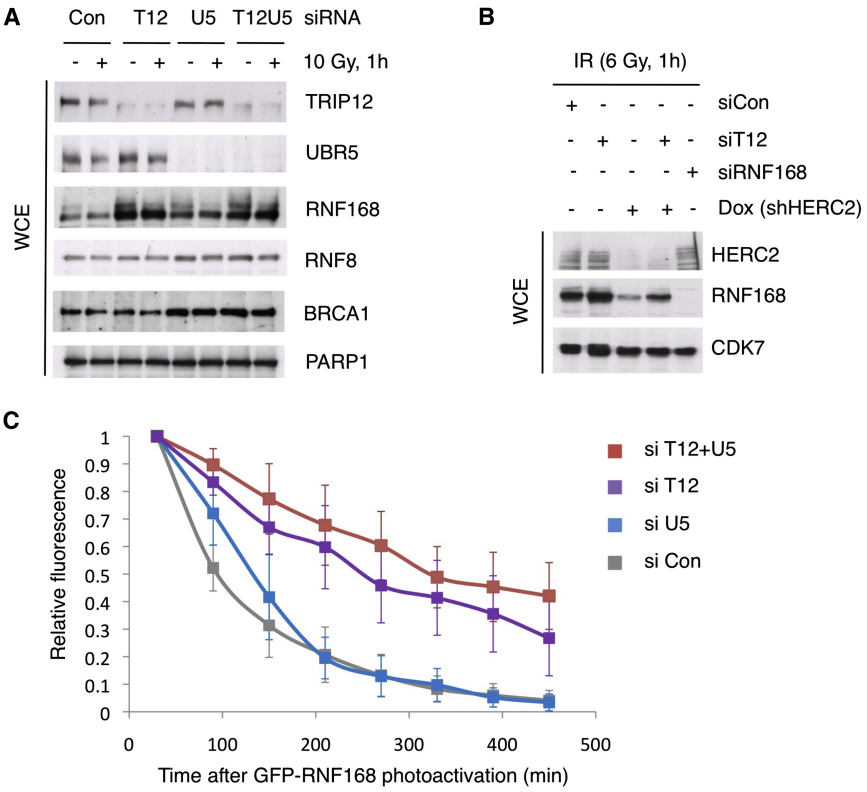

Figure 4. TRP12 and UBR5 Determine the Abundance and Chromatin Loading of RNF168

(A) U-2-OS cells were transfected with siRNA for 72 hr and irradiated as indicated. Whole-cell extracts (WCE) were analyzed by immunoblotting.

(B) U-2-OS cells conditionally expressing Dox-ycyclin (Dox)-inducible HERC2 shRNA were induced by incubating in the media with Dox for 120 hr. For the last 72 hr, cells were transfected with the indicated siRNAs. WCE were analyzed by immunoblotting with the indicated antibodies.

(C) U-2-OS cells stably expressing photo-activatable GFP-RNF168 were treated with the indicated siRNAs for 72 hr and photoactivated, and the GFP-associated fluorescence intensities were recorded at the indicated time points. The data represent background-subtracted fluores-cence intensities averaged from ten cells for each condition. Error bars represent SD.

(D) U-2-OS cells were transfected with siRNAs for 72 hr and irradiated as indicated. Chromatin-en-riched fractions were analyzed by immunoblotting.

(E) U-2-OS cells were transfected with expression plasmids for HA-RNF168 and HA-RNF8, respec-tively. After 24 hr, the cells were immunostained with an antibody to the hemagglutinin (HA) tag. Arrows mark the nuclear bodies occupied by the respective proteins. Nuclear DNA was stained by DAPI.

Scale bar, 10 μm. See also Figures S4 and S5.

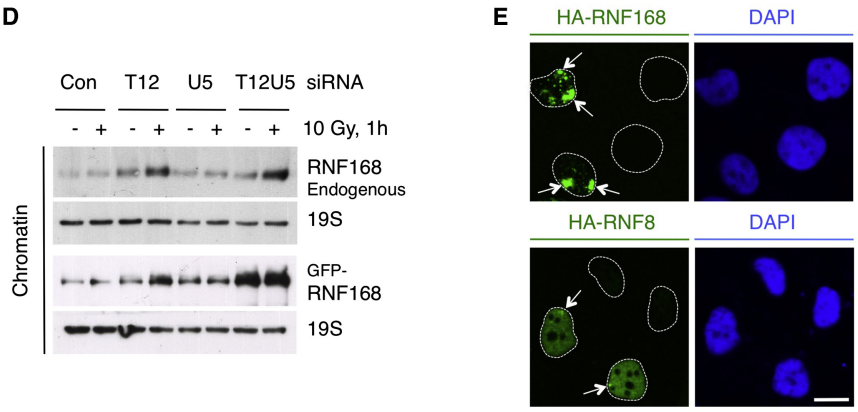

The Levels of RNF168 Render the Ubiquitin Signaling Rate Limiting

When combined, the previous results suggest that, due to its unique propen-sity to autoamplify (see Introduction), RNF168 might have evolved as the prime target for mechanisms that control the magnitude of DNA-damage-induced chromatin ubiquitylation. If true, it should be possible to generate conditions when the pool of endogenous RNF168 be-comes limiting. To test this, we used the TRIP12 and UBR5 knockdown as a molecular tool to maximally mobilize endogenous RNF168, exposed cells to increasing doses of IR (0.25–4 Gy), and quantified in hundreds of randomly chosen cells the magnitude of ubiquitin-dependent protein accumulations at damaged chromatin. As a readout, we again used 53BP1 because of the strict dependency of its chromatin accumulation on RNF168 (Doil et al., 2009; Stewart et al., 2009) and the fact that it is a fairly abundant protein whose levels were not changed by TRIP12 or UBR5 manipulations (Figure S5E).

Strikingly, naive U-2-OS cells and primary human fibroblasts responded to the increasing dose of IR by a progressive reduc-tion of fluorescence intensity and areas of nuclear foci occupied by 53BP1 (Figures 5A, S6A, and S6B). Although the sum of 53BP1 fluorescence associated with all IR-induced foci per

TRIP12- and UBR5-depleted cells (Figure S1D), and its knock-down did not prevent RNF168 stabilization (Figure S5D), sug-gesting that the regulation of the RNF168 protein abundance by TRIP12 and UBR5 is autonomous. However, depletion of RNF8 did impair DNA-damage-induced chromatin loading of RNF168 in TRIP12- and UBR5-depleted cells (Figures S3D and S5D). Together, these results suggest that, in the absence of TRIP12 and UBR5, the DSB-induced ubiquitylation path-way operates under the same principles as in normal cells with the exception that it is hyperactive; this includes unsched-uled RNF168 accumulation, its excessive loading on chromatin, and spreading of ubiquitin conjugates far away from the DNA lesions.

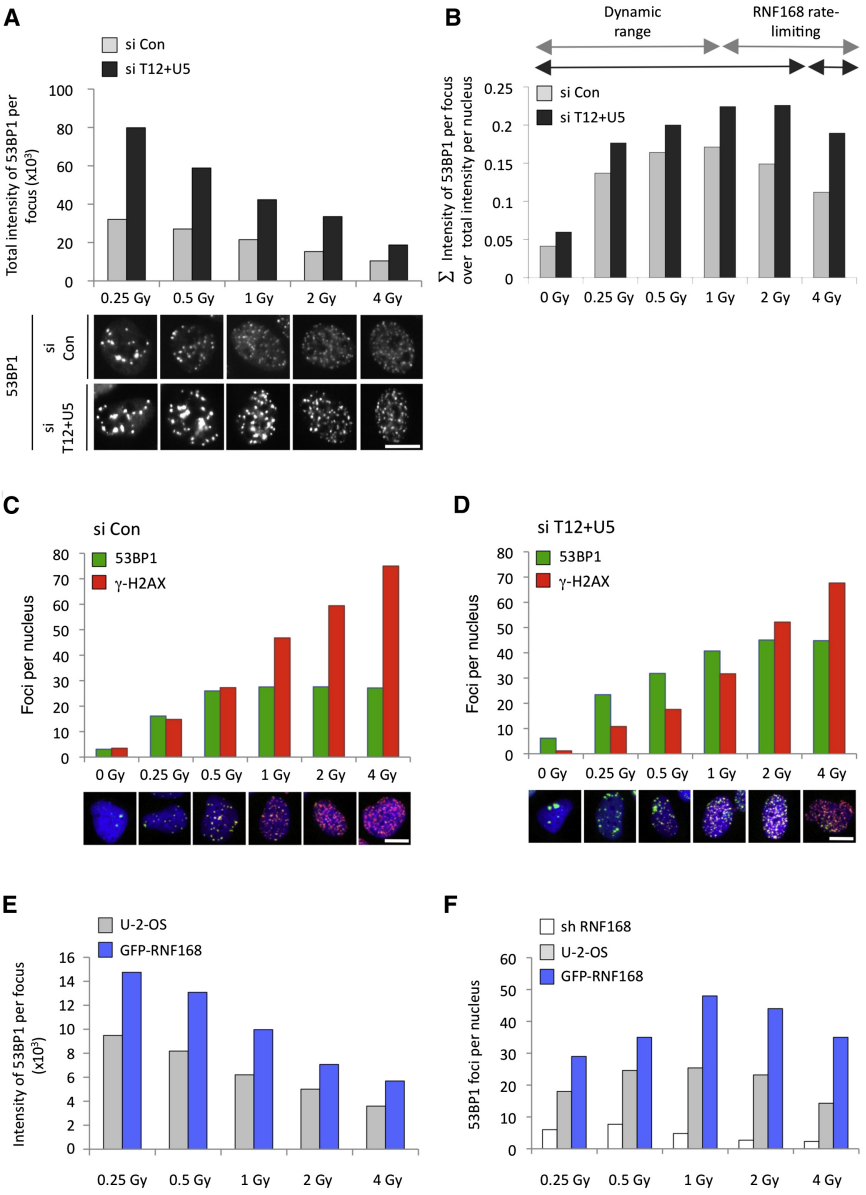

Figure 5. RNF168 Abundance Is Rate Limiting for 53BP1 Focus Formation

(A) U-2-OS cells were transfected with siRNAs for 72 hr and exposed to increasing doses of IR as indicated, and after 1 hr, they were immunostained with an antibody to 53BP1. Wide-field images were acquired from randomly selected fields. The graph shows the total fluorescence intensity per 53BP1-decorated nuclear focus. Representative images for each condition are shown. Scale bar, 10 μm.

(B) U-2-OS cells were transfected with siRNAs for 72 hr and irradiated as indicated, and 1 hr later, they were immunostained with an antibody to 53BP1. Wide-field images of 53BP1 were acquired from randomly selected fields. The graph shows the average sum of total fluorescence intensity associated with 53BP1 nuclear foci normalized to the total fluorescence intensity of 53BP1 per nucleus.

(C) U-2-OS were transfected with control siRNA and irradiated as indicated, and 1 hr later, they were immunostained with antibodies to 53BP1 and γ-H2AX. Wide-field images were acquired from randomly selected fields and analyzed for the number of nuclear foci per nucleus. Representative images are shown.

(D) U-2-OS cells were transfected with the TRIP12 and UBR5 siRNAs and analyzed as in (C).

(E) U-2-OS cells expressing GFP-RNF168 or naive U-2-OS cells were irradiated and analyzed for 53BP1-associated fluorescence as in (A).

(F) U-2-OS cells stably expressing GFP-RNF168, U-2-OS cell line induced to express RNF168 shRNA for 72 hr (used here as a negative control for suppression of 53BP1 focus formation), or naive U-2-OS cells were irradiated and analyzed for 53BP1 foci number. For each condition in (A)–(F), a randomly selected cohort of at least 500 cells was analyzed.

Scale bars, 10 μm. See also Figure S6.

nucleus increased up to 1–2 Gy (corresponding to 20–40 DSB), it began to decline at higher doses (Figure 5B). Together, these data suggest that, after exceeding a dynamic range defined by RNF168 abundance, the increasing amount of DNA breaks fails to induce productive chromatin ubiquitylation. Consistent with this conclusion, the absolute number of 53BP1 foci per nucleus increased only up to 1 Gy of IR (Figure 5C). Importantly, the number of γ-H2AX foci continued to rise throughout the entire dose range (Figure 5C), suggesting that the DNA-damage-induced ubiquitylation is an autonomous and rate-limiting pathway that, unlike histone phosphorylation, can be saturated by relatively low amounts of DSB.

Most importantly, the combined TRIP12/UBR5 knockdown elevated the threshold to higher IR doses at all assay levels, including the intensity, area, and number of 53BP1-decorated nuclear foci, respectively (Figures 5A, 5B, 5D, and S6B). To test whether this can be attributed to TRIP12/UBR5-mediated control of RNF168 abundance, we repeated these measurements in cells stably expressing ectopic GFP-RNF168 (Figure S6C). Under these conditions, we also observed enhancement of 53BP1-decorated chromatin areas (Figures 5E and S6D) and productive 53BP1 focus formation at higher doses (Figure 5F). We conclude that the cellular capacity to ubiquitylate chromatin after DNA breakage is limited and that the levels of RNF168 set a threshold, which determines the extent of this modification.

The RNF168 Threshold Determines the Dynamics of DSB Repair

To test the consequences of the threshold imposed by the TRIP12/UBR5-RNF168 crosstalk for DNA repair, we turned to one of the key functions of RNF168, namely its ability to recruit to the DSB-flanking chromatin various genome caretakers,

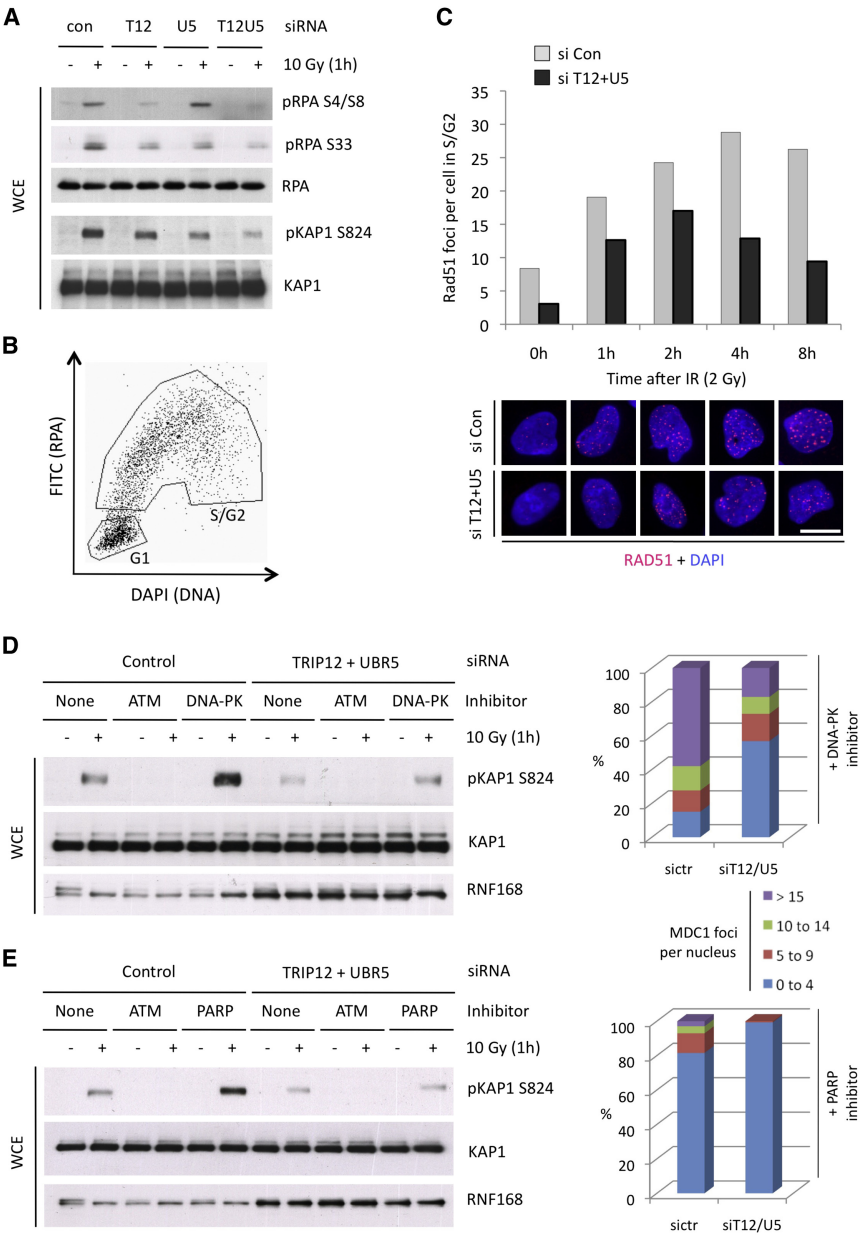

Figure 6. Deregulation of TRIP12 and UBR5 Alters the Dynamics of DNA Repair

(A) U-2-OS cells were transfected with the indicated siRNA for 72 hr and irradiated. WCE were analyzed by immunoblotting.

(B) U-2-OS cells were irradiated (2 Gy), and 1 hr later, they were immunostained with an antibody to RPA (the FITC channel); nuclear DNA was counterstained by DAPI. Cell-cycle distribution was determined for each individual cell by quantifying the total DAPI and chromatin-bound RPA intensity per nucleus.

(C) U-2-OS cells were transfected with the indicated siRNAs, irradiated, immunostained with antibodies to RPA and RAD51, sorted according to cell cycle as in (B), and subjected to an automated analysis of RAD51 focus formation. At least 500 cells were analyzed for each condition; representative images are shown.

(D) U-2-OS cells were transfected with siRNAs for 72 hr and irradiated. Where indicated, cells were treated for 2 hr with ATM or DNA-PK inhibitors prior to irradiation. WCE were analyzed by immunoblotting (left). In parallel, cells were treated with the indicated siRNAs and inhibitors as indicated, irradiated (2 Gy), and after 4 hr, were subjected to an automated single cell analysis for the number of MDC1 nuclear foci (right).

(E) U-2-OS cells were treated with the indicated siRNAs and inhibitors, irradiated, and analyzed as in (D).

Scale bar, 10 μm. See also Figure S7.

including proteins that influence DNA end processing (see Introduction). Indeed, we observed that depletion of TRIP12 and UBR5 cooperated in reducing phosphorylation of replication protein A (RPA), a surrogate of DSB resection (Figure 6A). This was, at least in part, mediated by elevated RNF168 because its simultaneous knockdown restored RPA phosphorylation (Figure S7A). Consistently, when we extended these assays obtained at a single time point by monitoring temporal dynamics of RAD51 focus formation, we observed a lower incidence and a more rapid clearance of RAD51 foci after TRIP12 and UBR5 depletion (Figures 6B and 6C). Thus, excessive chromatin ubiquitylation appears to trigger faster and/or more efficient DSB repair.

Several independent experiments supported this conclusion. Although TRIP12/UBR5 depletion did not generally affect IR-induced ATM autophosphorylation (Figure S7B), it caused a marked reduction of KAP1 phosphorylation (Figure 6A), and also, this effect appeared to be mediated by elevated RNF168 (Figure S7A). KAP1 is an ATM substrate whose phosphorylation correlates with slow DSB repair kinetics (Goodarzi et al., 2010). Consistently, we found that KAP1 phosphorylation increased when DSB repair by nonhomologous end-joining (NHEJ) was compromised (Figures 6D, 6E, and S7C). Strikingly, depletion of TRIP12 and UBR5 partially suppressed even this elevated KAP1 phosphorylation (Figures 6D and 6E), suggesting that the hyperaccumulation of RNF168 might rescue efficient DSB repair, even under these suboptimal conditions.

We validated and further extended these biochemical analyses by monitoring physiological parameters associated with DNA repair. First, we observed that the depletion of TRIP12 and UBR5 accelerated the disappearance of γ-H2AX and MDC1 repair foci both in naive U-2-OS cells (Figures S7D and S7E) and in cells with reduced activities of DNA-dependent protein kinase catalytic subunit (DNA-PK) or poly(ADP-ribose) polymerase (PARP) enzymes (Figures 6D and 6E). Second, by using reporter assays, we detected a significant increase of the NHEJ-directed repair (Figure 7A), which was consistent

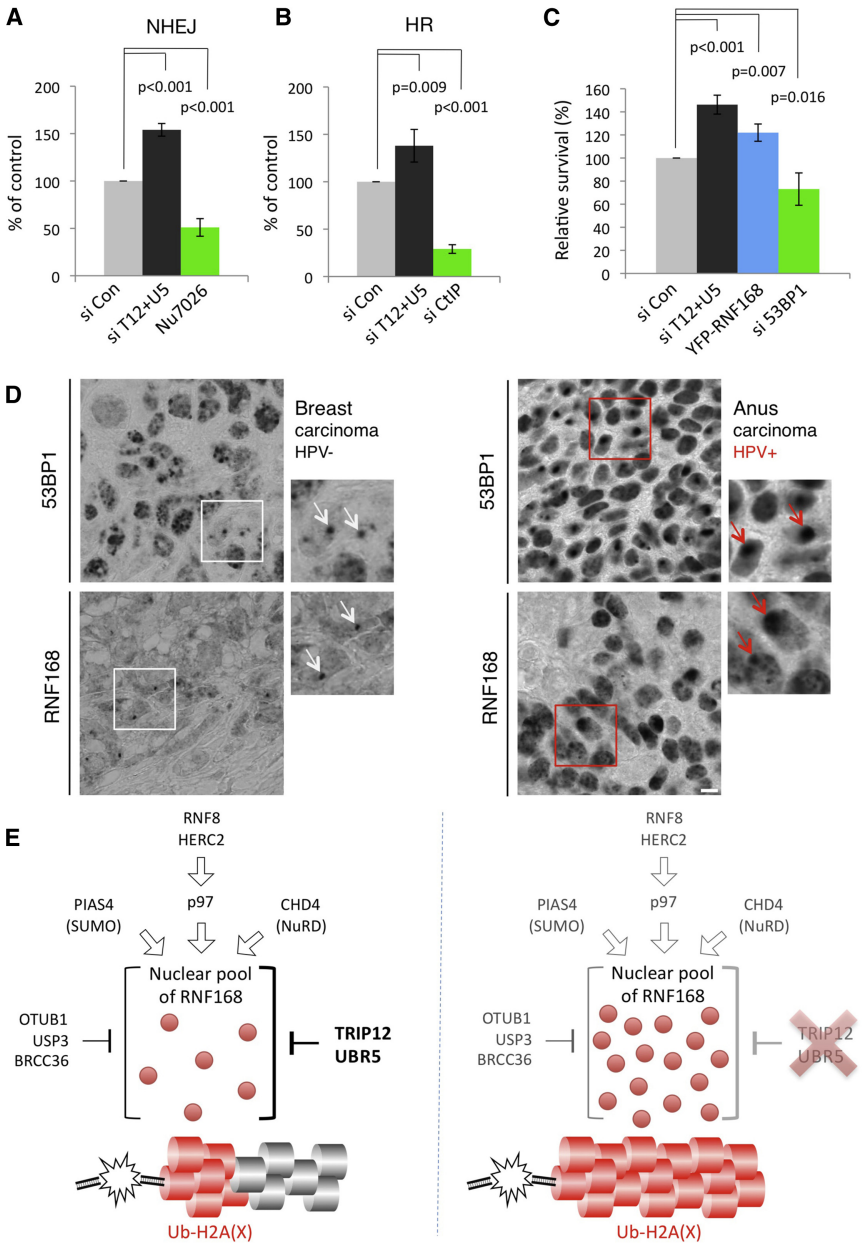

Figure 7. Mechanisms Determining RNF168 Turnover Influence Survival after DNA Damage and Can Be Deregulated in Human Cancer

(A) H1299 dA3-1 cells were transfected with indicated siRNAs for 24 hr, followed by transfection with a plasmid expressing I-SceI for 72 hr, and then they were harvested. Where indicated, DNA-PKcs inhibitor NU7026 was added to cells at the time of I-SceI transfection. The proportion of GFP-positive cells (as a measure of NHEJ activity) was determined by flow cytometry. Data represent the mean from three experiments.

(B) U-2-OS/DR-GFP cells were transfected with siRNAs as indicated and then cotransfected with expression plasmids for I-SceI and RFP for 48 hr. Flow cytometry analysis of GFP/RFP ratio was used to measure HR efficiency. Data represent the mean of five experiments.

(C) MCA survival assay. U-2-OS cells expressing GFP were cotransfected with TRIP12 and UBR5 siRNAs for 48 hr and mixed in a 1:1 ratio with a U-2-OS cell line expressing mCherry transfected with control siRNA. Where indicated, U-2-OS/YFP-RNF168 induced to express the transgene by addition of Doxycycline (Dox) were mixed with the U-2-OS/mCherry cells and processed as above. After an additional 24 hr, cells were irradiated (5 Gy) and were analyzed 72 hr later by flow cytometry. The survival was determined as the GFP/mCherry ratio. The data represent a summary from three experiments. Error bars in (A)–(C) represent SD.

(D) Paraffin sections from the indicated tumor types were immunostained with antibodies to 53BP1 or RNF168. Insets show larger magnifications of the marked fields; arrows point to nuclear bodies. The HPV status of the depicted tumors is indicated.

(E) Model of TRIP12/UBR5-mediated suppression of chromatin ubiquitylation after DNA breakage. Left, TRIP12 and UBR5 determine the nuclear pool of RNF168. This pool is under full control by the upstream regulators and is available to ubiquitylate a limited fraction of the DSB-flanking chromatin. Right, in the absence of TRIP12 and UBR5, a fraction of hyperaccumulated RNF168 escapes upstream regulators and triggers spreading of H2A and H2AX ubiquitylation far away from the initial DNA lesions.

Scale bar, 10 μm.

with the increased loading of RNF168 and 53BP1 on the damaged loci under these conditions. Of note, homology-directed repair was also elevated in TRIP12/UBR5-depleted cells (Figure 7B), suggesting a broader impact of protein quality control in DNA damage responses (see Discussion). Third, a multicolor competition assay (MCA) (Smogorzewska et al., 2007) revealed improved short-term survival after irradiation both in TRIP12/UBR5-depleted cells and in cells engineered to transiently increase the RNF168 pool from a conditional yellow fluorescent protein (YFP)-RNF168 transgene (Figure 7C). Importantly, depletion of 53BP1, the sensor of chromatin ubiquitylation, had an opposite effect and decreased cell survival under these conditions (Figure 7C). Together, these data suggest that boosting chromatin ubiquitylation enhances repair efficiency of clastogen-induced DSBs.

Elevated RNF168 and Expanded 53BP1 Nuclear Bodies Are Associated with Advanced HPV-Transformed Human Malignancies

In search for disease-associated aberrations of the described mechanisms, we noticed a recent study describing unusually large 53BP1 foci in advanced human papillomavirus (HPV)-positive cervical cancers (Matsuda et al., 2011). We revisited this issue and found that diverse HPV-positive tumor types contain markedly enlarged 53BP1 nuclear bodies, and more significantly, that this is accompanied by dramatically increased levels

of endogenous RNF168 (Figure 7D). Specifically, 50% (n = 20) of HPV-associated tumors showed expanded 53BP1 bodies and high levels of RNF168, whereas none (n = 40) of HPV-negative carcinomas showed these phenotypes. Among the HPV-associated tumors, the highest incidence of nuclear body expansion was detected in carcinomas of anus (five of six), followed by uterine cervix (four of eight) and rhinopharynx (one of six). Thus, although a detailed assessment of RNF168 gain of function in pathogenesis of human cancer awaits more dedicated studies, these results suggest that such a connection indeed exists and that the pathway described here could be subverted by transforming viruses such as the HPV.

DISCUSSION

Here, we uncovered a mechanism that provides three additions to the current concepts of chromatin responses to DNA breakage. First, we show that an excessive spreading of a DNA-damage-associated chromatin modification can occur. Second, we identified TRIP12 and UBR5 as two suppressors of such spreading. Third, our results indicate that the rate-limiting nature of chromatin ubiquitylation influences physiological consequences of genotoxic stress, such as the extent of transcriptional silencing, the dynamics of DSB repair pathways, and cell survival.

Our results can be integrated into the following model (Figure 7E): under physiological conditions, TRIP12 and UBR5 determine the size of the RNF168 nuclear pool, which dynamically responds to the plethora of upstream regulators and supports limited chromatin ubiquitylation confined to the vicinity of the DNA lesions. In the absence of TRIP12 and UBR5, RNF168 accumulates to supraphysiological levels, escapes the fine-tuning effect of upstream regulators, and triggers spreading of histone ubiquitylations away from the DSB sites. The salient feature of this model is that the excessive spreading of DNA-damage-induced ubiquitylation is not limited by physical ''insulators'' within the higher-order chromatin structure but is determined by the number of RNF168 molecules.

Mechanistically, the cooperative effect of TRIP12 and UBR5 in keeping the RNF168 levels within the desirable limit could resemble their yeast orthologs (UFD4 and UBR1, respectively) that synergize in degrading shared substrates by enhancing the processivity of ubiquitin chain formation (Hwang et al., 2009, 2010). However, our data suggest that mammalian TRIP12 and UBR5 cooperate in suppressing RNF168 at an additional level. Based on its strong and selective impact on the RNF168 protein levels, TRIP12 appears to be the prime E3 ligase, which monitors nuclear RNF168 and thus guards against excessive chromatin ubiquitylation. An interesting parallel comes from studies of TRIP12 in different biological settings, which showed that the ARF, BAF57, and APP-BP1 proteins are targeted for TRIP12-mediated proteolysis only when uncoupled from their physiological binding partners (Chen et al., 2010; Keppler and Archer, 2010; Park et al., 2008). Intriguingly, there is a precedent that RNF168 is destabilized in the absence of HERC2, one of its interacting proteins (Bekker-Jensen et al., 2010), and we show that this enhanced proteolysis can be suppressed by depleting TRIP12. In this regard, it is possible that TRIP12 may control RNF168 turnover also by targeting one of its interacting partners and thereby ''unshielding'' it from the proteolytic machinery.

The second, arguably more basic, level of regulation seems to be provided by UBR5, which has recently emerged as an integral component of the cotranslational protein surveillance machinery (Pegoraro et al., 2012). Indeed, we show that knockdown of UBR5 leads to a modest but reproducible increase of all E3 enzymes involved in the DNA damage ubiquitylation pathway (RNF8, RNF168, and BRCA1). Consequently, attenuation of such surveillance would inevitably prime cells to escape physiological regulatory cues and become exquisitely sensitive to events that enhance chromatin ubiquitylation. We envisage that other members of the UBR family of E3 ligases or additional factors involved in ubiquitin fusion degradation (Varshavsky, 2011) can also participate in preventing ''unscheduled spikes'' of histone ubiquitylations. If this were the case, it would be interesting to investigate whether this operates directly via RNF168 as described here or whether there are additional rate-limiting factors along the pathway. Our findings (e.g., Figure 5) that the chromatin ubiquitylation can still be saturated to some extent, even in cells with elevated RNF168, indicate that, especially after massive DSB formation, additional factors can become limiting.

In our experimental conditions, the dynamic range of chromatin ubiquitylation is saturated at IR doses that correspond to (maximally) 20–40 DSBs. Within that range, the TRIP12/UBR5-mediated control over RNF168 abundance effectively supports chromatin ubiquitylation of most DSBs. Because one consequence of chromatin ubiquitylation is the increased chromatin retention of 53BP1, a factor that promotes end joining and restrains resection of DNA ends (Bothmer et al., 2011; Bouwman et al., 2010; Bunting et al., 2010; Cao et al., 2009), the bulk of DSBs under these conditions are likely repaired by NHEJ, which is a conclusion that is supported by the enhanced NHEJ efficiency measured in a cell-based reporter assay. By contrast, once the extent of DNA damage overcomes the threshold, DSBs progressively lose the ability to induce histone ubiquitylation (and 53BP1 chromatin retention), which in turn may increase the incidence of abortive NHEJ attempts and render the DSB repair more dependent on homology-directed repair.

An interesting ramification of how chromatin ubiquitylation contributes to repair efficiency is our observation that the depletion of TRIP12 and UBR5 enhances both NHEJ and homologous recombination (HR) (albeit the latter to a lower extent). The stimulating effect on NHEJ is consistent with the recent results demonstrating that some of the key ubiquitin sensors at the DSB-modified chromatin, such as 53BP1, promote DNA end joining (Bunting et al., 2012; Introduction). In case of HR, the mechanism remains more elusive, but several scenarios come to mind. Most notably in this regard, the observation that the DSB-associated chromatin events shift both major repair mechanisms to the same direction is not unprecedented. A recent study (Galanty et al., 2009) showed that the depletion of the DSB-associated SUMO ligases (enzymes that operate directly on the RNF168 pathway) attenuates both NHEJ and HR. Translated to our experimental system, we envisage that, in addition to RNF168, TRIP12/UBR5-deficient cells accumulate other genome caretakers that allow more efficient HR. Such proteins

could affect specific loci and/or might be restricted to a defined stage of cell-cycle progression. For instance, because the enhanced chromatin ubiquitylation in TRIP12/UBR5-depleted cells entails hyperaccumulation of BRCA1, it is possible that, close to the G2/M transition, when the progressive chromatin condensation starts to displace NHEJ factors such as 53BP1, the high local concentration of BRCA1 can facilitate HR of hitherto unresolved DSBs.

Aberrations of both TRIP12 and UBR5 have been reported in several types of human malignancies (Clancy et al., 2003; O'Brien et al., 2008; Yoo et al., 2011), and it is possible that excessive chromatin ubiquitylation in such cases might contribute to cancer progression. Although a systematic analysis of how chromatin hyperubiquitylation contributes to cancer development requires dedicated studies, our results identified at least two areas that may serve as useful leads in this effort. First, the increased survival in RNF168 overproducing cells could provide selective advantage to cancer cells that intrinsically proliferate under increased genotoxic stress (Bartkova et al., 2005). Second, the high incidence of elevated RNF168 and expanded 53BP1 chromatin domains in HPV-transformed tumors indicates that, in addition to the downregulation of RNF8 and RNF168 triggered by herpes-virus-encoded proteins (Lilley et al., 2010), oncogenic viruses could have evolved an alternative strategy and could subvert this pathway to expand the life span of host cells. The HPV-encoded E6 oncoprotein is a founder of the HECT domain E3 ligases, and it is intriguing to speculate that one way it subverts the host cell metabolism is via competing out cellular enzymes of the same family, including TRIP12 and UBR5.

EXPERIMENTAL PROCEDURES

DNA, RNA, and Transfections

A plasmid containing the full-length complementary DNA (cDNA) for human TRIP12 was obtained from Source BioScience (cloneIRCMp5012E0132D; transcript ENST 00000389044, Ensembl release 66) and was subcloned into the pAc-GFP-C1 vector (Clontech). The catalytically inactive version of TRIP12 (*HECT; C2007A) was generated by using the QuickChange Site-Directed Mutagenesis Kit (Stratagene). Full-length, untagged UBR5 cDNA was subcloned into pDNR221 from pEGFP-C1_EDD (Henderson et al., 2002). Catalytically inactive UBR5 *HECT (C2768A) was generated by replacing a C-terminal fragment of the wild-type (WT) cDNA with a synthetic sequence. Both WT and mutant UBR5 cDNA were cloned into pcDNA6.2/N-EmGFP-DEST (V356-20, Invitrogen). Plasmids for RNF8 and RNF168 were described (Doil et al., 2009; Mailand et al., 2007). The TetR-GFP plasmid was a gift from E. Soutoglou. Photoactivatable GFP plasmid was provided by J. Lipincott-Schwartz. Plasmid transfections were performed with the Lipofectamine LTX with Plus Reagent (Invitrogen). siRNA transfections were performed with siRNA duplexes (25 nM) by using Lipofectamine RNAiMAX (Invitrogen). For siRNA specificity, see Figure S2.

Cell Culture and Generation of DSBs

Human U-2-OS osteosarcoma cells, primary BJ fibroblasts and HEK293T cells, were grown in Dulbecco's modified Eagle's medium (DMEM) containing 10% fetal bovine serum (GIBCO). U-2-OS cell lines expressing GFP-RNF168, GFP-53BP1, a Doxycycline-inducible small hairpin RNA (shRNA) to RNF168, and a Doxycycline-inducible shRNA to HERC2 were described (Doil et al., 2009; Bekker-Jensen et al., 2010). U-2-OS cell lines with Doxycycline-inducible YFP-RNF168 or constitutively expressed photoactivatable GFP-RNF168, free GFP, and free mCherry, respectively, were generated by standard protocols (Bekker-Jensen et al., 2005; Lukas et al., 2004). Similar procedures were used to generate a U-2-OS cell line with stably integrated I-SceI restriction site flanked by 240 TetO repeats (Lau et al., 2003). Primary BJ fibroblasts were obtained from ATCC. X-ray irradiation was done with a XYLON.SMART 160E/1.5 device (150kV, 6 mA; YXLON International A/S, Taastrup, Denmark) delivering 11.8 mGy per second. Soft X-rays were largely filtered out with a 3 mm aluminum filter. Chemical inhibitors of PARP (ABT888, 10 μM), ATM (Kudos 55933, 10 μM), and DNA-PK (NU7441, 2 μM) were used. The multicolor competition assay was done as described (Smogorzewska et al., 2007); the results in Figure 7C were reproduced after swapping the recipient cell lines (GFP and mCherry, respectively) for the siRNA treatments. NHEJ and HR reporter assays were described (Poulsen et al., 2012).

Microscopy and Image Analysis

Automated wide-field microscopy was performed on an Olympus ScanR system (motorized IX81 microscope) with ScanR Image Acquisition Software and 20×/0.75 NA (UPLSAPO20×) and 40×/0.9 NA (UPLSAPO 40×) dry objectives, a quadruple-band filter set for Dapi, FITC, Cy3 and Cy5 fluorescent dyes, an MT20 Illumination system, and a digital monochrome Hamamatsu C9100 electron multiplying (EM)-charge-coupled device (CCD) camera. Confocal microscopy was performed on an LSM-510 (Carl Zeiss Microimaging Inc.) mounted on an upright Zeiss-Axioimager with an oil immersion objective (Plan-Apochromat 40×/1.3). Time-lapse microscopy was performed on AxioOserver.Z1 wide-field microscope (Carl Zeiss Microimaging Inc.) with a 40× oil immersion objective (Plan-Apochromat), a CCD camera (Coolsnap HQ, Roper Scientific), motorized stage, and fast shutters (Sutter Instruments). See also Extended Experimental Procedures.

Statistical Analysis

Differences in repair and survival assays were analyzed by Student's t test.

Data Online

Original images of the GFP-RNF168 screen (Figure 1B and Table S1) are deposited in the Mitocheck database (http://www.mitocheck.org/cgi-bin/mtc).

SUPPLEMENTAL INFORMATION

Supplemental Information includes Extended Experimental Procedures, seven figures, and one table and can be found with this article online at http://dx.doi.org/10.1016/j.cell.2012.06.039.

ACKNOWLEDGMENTS

We thank D. Durocher, X. Yu, T. Halazonetis, E. Soutoglou, J. Lippincott Schwartz, S. Watanabe, T. Kohno, and R. Strauss for reagents and technical advice, and we thank members of the Center Genotoxic Stress Research for helpful discussions. This work was supported by the Danish Cancer Society, the Danish National Research Foundation, the Lundbeck Foundation (R44-A4400), the Novo Nordisk Foundation, the Danish Council for Independent Research—Medical Sciences, the John and Birthe Meyer Foundation, European Commission (DDR Response, Biomedreg, and Infla-Care), Cancer Institute NSW, and the NSW Office of Science and Medical Research. M.A., L.T., and C.D. are recipients of long-term EMBO fellowships. Special thanks go to Jan Ellenberg, Rainer Pepperkok, and the Advanced Light Microscopy Facility (ALMF) at EMBL, Heidelberg, for generously supporting this project and for providing the siRNA arrays.

Received: January 12, 2012
Revised: April 26, 2012
Accepted: June 10, 2012
Published online: August 9, 2012

REFERENCES

Acs, K., Luijsterburg, M.S., Ackermann, L., Salomons, F.A., Hoppe, T., and Dantuma, N.P. (2011). The AAA-ATPase VCP/p97 promotes 53BP1 recruitment by removing L3MBTL1 from DNA double-strand breaks. Nat. Struct. Mol. Biol. *18*, 1345–1350.

Bartkova, J., Horejsí, Z., Koed, K., Krämer, A., Tort, F., Zieger, K., Guldberg, P., Sehested, M., Nesland, J.M., Lukas, C., et al. (2005). DNA damage response as a candidate anti-cancer barrier in early human tumorigenesis. Nature *434*, 864–870.

Bekker-Jensen, S., Lukas, C., Melander, F., Bartek, J., and Lukas, J. (2005). Dynamic assembly and sustained retention of 53BP1 at the sites of DNA damage are controlled by Mdc1/NFBD1. J. Cell Biol. *170*, 201–211.

Bekker-Jensen, S., Rendtlew Danielsen, J., Fugger, K., Gromova, I., Nerstedt, A., Lukas, C., Bartek, J., Lukas, J., and Mailand, N. (2010). HERC2 coordinates ubiquitin-dependent assembly of DNA repair factors on damaged chromosomes. Nat. Cell. Biol. *12*, 80–86.

Bothmer, A., Robbiani, D.F., Feldhahn, N., Gazumyan, A., Nussenzweig, A., and Nussenzweig, M.C. (2010). 53BP1 regulates DNA resection and the choice between classical and alternative end joining during class switch recombination. J. Exp. Med. *207*, 855–865.

Bothmer, A., Robbiani, D.F., Di Virgilio, M., Bunting, S.F., Klein, I.A., Feldhahn, N., Barlow, J., Chen, H.T., Bosque, D., Callen, E., et al. (2011). Regulation of DNA end joining, resection, and immunoglobulin class switch recombination by 53BP1. Mol. Cell *42*, 319–329.

Bouwman, P., Aly, A., Escandell, J.M., Pieterse, M., Bartkova, J., van der Gulden, H., Hiddingh, S., Thanasoula, M., Kulkarni, A., Yang, Q., et al. (2010). 53BP1 loss rescues BRCA1 deficiency and is associated with triple-negative and BRCA-mutated breast cancers. Nat. Struct. Mol. Biol. *17*, 688–695.

Bunting, S.F., Callén, E., Wong, N., Chen, H.T., Polato, F., Gunn, A., Bothmer, A., Feldhahn, N., Fernandez-Capetillo, O., Cao, L., et al. (2010). 53BP1 inhibits homologous recombination in Brca1-deficient cells by blocking resection of DNA breaks. Cell *141*, 243–254.

Bunting, S.F., Callen, E., Kozak, M.L., Kim, J.M., Wong, N., Lopez-Contreras, A.J., Ludwig, T., Baer, R., Faryabi, R.B., Malhowski, A., et al. (2012). BRCA1 functions independently of homologous recombination in DNA interstrand crosslink repair. Mol. Cell *46*, 125–135.

Cao, L., Xu, X., Bunting, S.F., Liu, J., Wang, R.H., Cao, L.L., Wu, J.J., Peng, T.N., Chen, J., Nussenzweig, A., et al. (2009). A selective requirement for 53BP1 in the biological response to genomic instability induced by Brca1 deficiency. Mol. Cell *35*, 534–541.

Chen, D., Shan, J., Zhu, W.G., Qin, J., and Gu, W. (2010). Transcription-independent ARF regulation in oncogenic stress-mediated p53 responses. Nature *464*, 624–627.

Clancy, J.L., Henderson, M.J., Russell, A.J., Anderson, D.W., Bova, R.J., Campbell, I.G., Choong, D.Y., Macdonald, G.A., Mann, G.J., Nolan, T., et al. (2003). EDD, the human orthologue of the hyperplastic discs tumour suppressor gene, is amplified and overexpressed in cancer. Oncogene *22*, 5070–5081.

Coleman, K.A., and Greenberg, R.A. (2011). The BRCA1-RAP80 complex regulates DNA repair mechanism utilization by restricting end resection. J. Biol. Chem. *286*, 13669–13680.

Doil, C., Mailand, N., Bekker-Jensen, S., Menard, P., Larsen, D.H., Pepperkok, R., Ellenberg, J., Panier, S., Durocher, D., Bartek, J., et al. (2009). RNF168 binds and amplifies ubiquitin conjugates on damaged chromosomes to allow accumulation of repair proteins. Cell *136*, 435–446.

Galanty, Y., Belotserkovskaya, R., Coates, J., Polo, S., Miller, K.M., and Jackson, S.P. (2009). Mammalian SUMO E3-ligases PIAS1 and PIAS4 promote responses to DNA double-strand breaks. Nature *462*, 935–939.

Goodarzi, A.A., Jeggo, P., and Lobrich, M. (2010). The influence of heterochromatin on DNA double strand break repair: getting the strong, silent type to relax. DNA Repair (Amst.) *9*, 1273–1282.

Harrigan, J.A., Belotserkovskaya, R., Coates, J., Dimitrova, D.S., Polo, S.E., Bradshaw, C.R., Fraser, P., and Jackson, S.P. (2011). Replication stress induces 53BP1-containing OPT domains in G1 cells. J. Cell Biol. *193*, 97–108.

Henderson, M.J., Russell, A.J., Hird, S., Muñoz, M., Clancy, J.L., Lehrbach, G.M., Calanni, S.T., Jans, D.A., Sutherland, R.L., and Watts, C.K. (2002). EDD, the human hyperplastic discs protein, has a role in progesterone receptor coactivation and potential involvement in DNA damage response. J. Biol. Chem. *277*, 26468–26478.

Henderson, M.J., Munoz, M.A., Saunders, D.N., Clancy, J.L., Russell, A.J., Williams, B., Pappin, D., Khanna, K.K., Jackson, S.P., Sutherland, R.L., and Watts, C.K. (2006). EDD mediates DNA damage-induced activation of CHK2. J. Biol. Chem. *281*, 39990–40000.

Hu, Y., Scully, R., Sobhian, B., Xie, A., Shestakova, E., and Livingston, D.M. (2011). RAP80-directed tuning of BRCA1 homologous recombination function at ionizing radiation-induced nuclear foci. Genes Dev. *25*, 685–700.

Hwang, C.S., Shemorry, A., and Varshavsky, A. (2009). Two proteolytic pathways regulate DNA repair by cotargeting the Mgt1 alkylguanine transferase. Proc. Natl. Acad. Sci. USA *106*, 2142–2147.

Hwang, C.S., Shemorry, A., Auerbach, D., and Varshavsky, A. (2010). The N-end rule pathway is mediated by a complex of the RING-type Ubr1 and HECT-type Ufd4 ubiquitin ligases. Nat. Cell Biol. *12*, 1177–1185.

Keppler, B.R., and Archer, T.K. (2010). Ubiquitin-dependent and ubiquitin-independent control of subunit stoichiometry in the SWI/SNF complex. J. Biol. Chem. *285*, 35665–35674.

Lau, I.F., Filipe, S.R., Søballe, B., Økstad, O.A., Barre, F.X., and Sherratt, D.J. (2003). Spatial and temporal organization of replicating Escherichia coli chromosomes. Mol. Microbiol. *49*, 731–743.

Lilley, C.E., Chaurushiya, M.S., Boutell, C., Landry, S., Suh, J., Panier, S., Everett, R.D., Stewart, G.S., Durocher, D., and Weitzman, M.D. (2010). A viral E3 ligase targets RNF8 and RNF168 to control histone ubiquitination and DNA damage responses. EMBO J. *29*, 943–955.

Lukas, C., Melander, F., Stucki, M., Falck, J., Bekker-Jensen, S., Goldberg, M., Lerenthal, Y., Jackson, S.P., Bartek, J., and Lukas, J. (2004). Mdc1 couples DNA double-strand break recognition by Nbs1 with its H2AX-dependent chromatin retention. EMBO J. *23*, 2674–2683.

Lukas, C., Savic, V., Bekker-Jensen, S., Doil, C., Neumann, B., Pedersen, R.S., Grøfte, M., Chan, K.L., Hickson, I.D., Bartek, J., and Lukas, J. (2011a). 53BP1 nuclear bodies form around DNA lesions generated by mitotic transmission of chromosomes under replication stress. Nat. Cell Biol. *13*, 243–253.

Lukas, J., Lukas, C., and Bartek, J. (2011b). More than just a focus: The chromatin response to DNA damage and its role in genome integrity maintenance. Nat. Cell Biol. *13*, 1161–1169.

Mailand, N., Bekker-Jensen, S., Faustrup, H., Melander, F., Bartek, J., Lukas, C., and Lukas, J. (2007). RNF8 ubiquitylates histones at DNA double-strand breaks and promotes assembly of repair proteins. Cell *131*, 887–900.

Matsuda, K., Miura, S., Kurashige, T., Suzuki, K., Kondo, H., Ihara, M., Nakajima, H., Masuzaki, H., and Nakashima, M. (2011). Significance of p53-binding protein 1 nuclear foci in uterine cervical lesions: endogenous DNA double strand breaks and genomic instability during carcinogenesis. Histopathology *59*, 441–451.

Meerang, M., Ritz, D., Paliwal, S., Garajova, Z., Bosshard, M., Mailand, N., Janscak, P., Hübscher, U., Meyer, H., and Ramadan, K. (2011). The ubiquitin-selective segregase VCP/p97 orchestrates the response to DNA double-strand breaks. Nat. Cell Biol. *13*, 1376–1382.

Moudry, P., Lukas, C., Macurek, L., Neumann, B., Heriche, J.K., Pepperkok, R., Ellenberg, J., Hodny, Z., Lukas, J., and Bartek, J. (2012). Nucleoporin NUP153 guards genome integrity by promoting nuclear import of 53BP1. Cell Death Differ. *19*, 798–807.

Munoz, M.A., Saunders, D.N., Henderson, M.J., Clancy, J.L., Russell, A.J., Lehrbach, G., Musgrove, E.A., Watts, C.K., and Sutherland, R.L. (2007). The E3 ubiquitin ligase EDD regulates S-phase and G(2)/M DNA damage checkpoints. Cell Cycle *6*, 3070–3077.

Nakada, S., Tai, I., Panier, S., Al-Hakim, A., Iemura, S., Juang, Y.C., O'Donnell, L., Kumakubo, A., Munro, M., Sicheri, F., et al. (2010). Non-canonical inhibition of DNA damage-dependent ubiquitination by OTUB1. Nature *466*, 941–946.

Nicassio, F., Corrado, N., Vissers, J.H., Areces, L.B., Bergink, S., Marteijn, J.A., Geverts, B., Houtsmuller, A.B., Vermeulen, W., Di Fiore, P.P., and Citterio, E. (2007). Human USP3 is a chromatin modifier required for S phase progression and genome stability. Curr. Biol. *17*, 1972–1977.

O'Brien, P.M., Davies, M.J., Scurry, J.P., Smith, A.N., Barton, C.A., Henderson, M.J., Saunders, D.N., Gloss, B.S., Patterson, K.I., Clancy, J.L., et al. (2008). The E3 ubiquitin ligase EDD is an adverse prognostic factor for serous epithelial ovarian cancer and modulates cisplatin resistance in vitro. Br. J. Cancer *98*, 1085–1093.

Park, Y., Yoon, S.K., and Yoon, J.B. (2008). TRIP12 functions as an E3 ubiquitin ligase of APP-BP1. Biochem. Biophys. Res. Commun. *374*, 294–298.

Pegoraro, G., Voss, T.C., Martin, S.E., Tuzmen, P., Guha, R., and Misteli, T. (2012). Identification of mammalian protein quality control factors by high-throughput cellular imaging. PLoS ONE *7*, e31684.

Peuscher, M.H., and Jacobs, J.L. (2011). DNA-damage response and repair activities at uncapped telomeres depend on RNF8. Nat. Cell Biol. *13*, 1139–1145.

Pinato, S., Gatti, M., Scandiuzzi, C., Confalonieri, S., and Penengo, L. (2011). UMI, a novel RNF168 ubiquitin binding domain involved in the DNA damage signaling pathway. Mol. Cell. Biol. *31*, 118–126.

Poulsen, M., Lukas, C., Lukas, J., Bekker-Jensen, S., and Mailand, N. (2012). Human RNF169 is a negative regulator of the ubiquitin-dependent response to DNA double-strand breaks. J. Cell Biol. *197*, 189–199.

Shanbhag, N.M., Rafalska-Metcalf, I.U., Balane-Bolivar, C., Janicki, S.M., and Greenberg, R.A. (2010). ATM-dependent chromatin changes silence transcription in cis to DNA double-strand breaks. Cell *141*, 970–981.

Shao, G., Lilli, D.R., Patterson-Fortin, J., Coleman, K.A., Morrissey, D.E., and Greenberg, R.A. (2009). The Rap80-BRCC36 de-ubiquitinating enzyme complex antagonizes RNF8-Ubc13-dependent ubiquitination events at DNA double strand breaks. Proc. Natl. Acad. Sci. USA *106*, 3166–3171.

Smogorzewska, A., Matsuoka, S., Vinciguerra, P., McDonald, E.R., III, Hurov, K.E., Luo, J., Ballif, B.A., Gygi, S.P., Hofmann, K., D'Andrea, A.D., and Elledge, S.J. (2007). Identification of the FANCI protein, a monoubiquitinated FANCD2 paralog required for DNA repair. Cell *129*, 289–301.

Stewart, G.S., Panier, S., Townsend, K., Al-Hakim, A.K., Kolas, N.K., Miller, E.S., Nakada, S., Ylanko, J., Olivarius, S., Mendez, M., et al. (2009). The RIDDLE syndrome protein mediates a ubiquitin-dependent signaling cascade at sites of DNA damage. Cell *136*, 420–434.

Varshavsky, A. (2011). The N-end rule pathway and regulation by proteolysis. Protein Sci. *20*, 1298–1345.

Yoo, N.J., Park, S.W., and Lee, S.H. (2011). Frameshift mutations of ubiquitination-related genes HERC2, HERC3, TRIP12, UBE2Q1 and UBE4B in gastric and colorectal carcinomas with microsatellite instability. Pathology *43*, 753–755.